

¹⁸F-FDG as an inflammation biomarker for imaging dengue virus infection and treatment response

Ann-Marie Chacko,¹ Satoru Watanabe,² Keira J. Herr,¹ Shirin Kalimuddin,³ Jing Yang Tham,¹ Joanne Ong,¹ Marie Reolo,¹ Raymond M.F. Serrano,¹ Yin Bun Cheung,^{4,5} Jenny G.H. Low,³ and Subhash G. Vasudevan²

¹Laboratory for Translational and Molecular Imaging, Cancer and Stem Cell Biology Programme, and ²Programme in Emerging Infectious Disease, Duke-NUS Medical School, Singapore. ³Department of Infectious Diseases, Singapore General Hospital, Singapore. ⁴Centre for Quantitative Medicine, Duke-NUS Medical School, Singapore. ⁵Center for Child Health Research, University of Tampere and Tampere University Hospital, Tampere, Finland.

Development of antiviral therapy against acute viral diseases, such as dengue virus (DENV), suffers from the narrow window of viral load detection in serum during onset and clearance of infection and fever. We explored a biomarker approach using ¹⁸F-fluorodeoxyglucose (¹⁸F-FDG) PET in established mouse models for primary and antibody-dependent enhancement infection with DENV. ¹⁸F-FDG uptake was most prominent in the intestines and correlated with increased virus load and proinflammatory cytokines. Furthermore, a significant temporal trend in ¹⁸F-FDG uptake was seen in intestines and selected tissues over the time course of infection. Notably, ¹⁸F-FDG uptake and visualization by PET robustly differentiated treatment-naïve groups from drug-treated groups as well as nonlethal from lethal infections with a clinical strain of DENV2. Thus, ¹⁸F-FDG may serve as a novel DENV infection-associated inflammation biomarker for assessing treatment response during therapeutic intervention trials.

Introduction

Acute infections caused by dengue virus (DENV) and other members of the flavivirus genus, such as Zika virus, Japanese encephalitis virus, West Nile virus, and yellow fever virus, pose a significant threat to global public health (1, 2). The four related dengue viral serotypes (DENV1–DENV4) cause a diversity of clinical manifestations, from mild, self-limiting dengue fever (DF) to severe and potentially fatal dengue hemorrhagic fever (DHF) or dengue shock syndrome (DSS). DHF and DSS usually occur during secondary heterotypic infections, through mechanisms such as the proposed antibody-dependent enhancement (ADE) (3–6). Owing to its high economic cost and public health burden, there is an urgent unmet need for therapeutics against DENV. The first preventative dengue vaccine, Dengvaxia (CYD-TDV, Sanofi Pasteur), has only recently been licensed for clinical use. This is despite strong reservations about its public health value, because the protective efficacy among vaccinated seronegatives was low, while among vaccinated seropositives, the efficacy was higher (7, 8).

There is limited information on DENV-infected human tissue biopsies, since postmortems are rarely conducted on mortality cases (9). Serum viral load (viremia), the current clinical diagnostic gold standard, does not always correlate with disease severity, nor does it robustly inform to anti-dengue therapy response under strict clinical trial conditions (10–12). However, DENV infection is consistently associated with cells of the mononuclear phagocyte lineage, and their increased proinflammatory cytokine production is believed to enhance disease severity by disrupting the integrity of vascular endothelial lining and causing increased vascular permeability (13, 14). A comprehensive review comparing preclinical animal models used in dengue pathogenesis research has been recently compiled (15). The AG129 mouse model, which is deficient in IFN- α , - β , and - γ , has been used extensively to recapitulate some of the salient features of lethal human diseases, such as high viremia level, elevated cytokine levels, vascular leakage, and thrombocytopenia (16–19). We recently showed that the infection of AG129 mice with mouse-adapted S221 DENV2/anti-DENV envelope glycoprotein monoclonal antibody immune complexes resulted in a tissue-

Authorship note: A.M. Chacko and S. Watanabe contributed equally to this work.

Conflict of interest: The authors have declared that no conflict of interest exists.

Submitted: February 17, 2017

Accepted: April 4, 2017

Published: May 4, 2017

Reference information:

JCI Insight. 2017;2(9):e93474. <https://doi.org/10.1172/jci.insight.93474>.

specific increase of viral load and inflammatory cytokines, such as IL-6 and TNF- α . Consequently, the mice were treated with anti-TNF antibody, after which they achieved a 100% recovery (20). Furthermore, several examples of nonlethal (virus-only) or lethal ADE infection of AG129 mice with clinical isolates of DENV have been reported, which share disease features that center around inflammation (11, 18, 19, 21). Viremia did not necessarily correlate with disease severity in many of these models (22), and the viral inoculum used in these infection studies also varied. Since lethality can be induced by both mouse-adapted and clinical strains, we hypothesized that a biomarker that could accurately reflect viral replication activity and immunopathogenesis, by tracking the associated inflammatory changes, may provide a valuable translational paradigm to study the effects of novel anti-dengue strategies.

The radiotracer ^{18}F -fluorodeoxyglucose (^{18}F -FDG) is widely used in clinical medicine for noninvasive imaging, staging, and monitoring treatment responses of neoplastic diseases (23). ^{18}F -FDG has also been used to nonspecifically image sites of viral infection or inflammation, because its detection can be proportional to the glycolytic activity of the cells that trap it (24–26). In this preclinical study, we demonstrate the efficacy of ^{18}F -FDG-based PET combined with CT imaging (^{18}F -FDG-PET/CT) as a noninvasive imaging strategy for the sensitive detection of inflammatory disease foci in dengue-infected mice and for monitoring disease amelioration in response to treatment.

Results

Lethal mouse-adapted DENV infection results in strong intestinal ^{18}F -FDG uptake. To explore the use of ^{18}F -FDG as a surrogate biomarker, we initially used the lethal ADE infection model on mouse-adapted S221 DENV2 (20), in which acute tissue-specific viral and inflammatory signatures were observed in small and large intestines (S.Int. and L.Int., respectively). Following the schematic in Figure 1A, we tracked DENV disease progression by postmortem assessment of virus and cytokine profiles and ^{18}F -FDG organ biodistribution. Finally, in vivo longitudinal ^{18}F -FDG PET/CT imaging was conducted for noninvasive whole-body detection of ^{18}F -FDG lesions.

Postmortem ^{18}F -FDG tissue biodistribution, with tissue uptake expressed as the percentage of injected dose per gram of tissue (%ID/g), increased significantly ($P < 0.001$), relative to noninfected mice. Over a 4-day course of DENV infection, the tissue uptake ratios of infected versus noninfected mice for the S.Int., L.Int., and spleen were 13.2, 2.8, and 4.8, respectively (Figure 1B), after which mice were moribund. ^{18}F -FDG uptake in lung, kidney, brain, and, notably, the liver was not substantially different throughout disease progression (Supplemental Table 1; supplemental material available online with this article; <https://doi.org/10.1172/jci.insight.93474DS1>). For ^{18}F -FDG to be a valid biomarker of dengue infection, we expected the uptake to show a statistically significant temporal trend, although the exact trajectory in different tissues is unknown. Fitting fractional polynomial regression models to the data, a nonlinear trend was found in each of the tissues assessed, each $P < 0.001$ against the null hypothesis of no trend and best fitting linear trend (Figure 1B). In particular, for the S.Int. and L.Int., there was a trough around day 2 after infection because of a sharp increase in ^{18}F -FDG uptake on days 3 and 4. The reasons for the trough remain to be understood.

Next, ^{18}F -FDG uptake of key inflamed and noninflamed tissues was assessed against virus replication (tissue viral load) (Figure 1C) and levels of signature inflammatory cytokines IL-6 and TNF- α (Figure 1, D and E). ^{18}F -FDG uptake in the spleen was not correlated with viral RNA and TNF- α . In the liver, a highly investigated site of viral replication in preclinical models, ^{18}F -FDG uptake only loosely correlated with viral load at higher viral titers (Spearman's $\rho = 0.67$, $P < 0.001$). Liver uptake also poorly correlated with cytokine markers, given the small dynamic range of cytokine expression levels (IL-6, Spearman's $\rho = 0.47$, $P < 0.05$; TNF- α , Spearman's $\rho = 0.23$, NS). A much stronger correlation was observed in the intestines between ^{18}F -FDG uptake and all three biomarkers (Spearman's $\rho = 0.77$ – 0.92 , $P < 0.0001$), with that of IL-6 in the S.Int. being the strongest.

Serial ^{18}F -FDG-PET/CT imaging within the same animal infected with lethal S221 DENV2 revealed prominent progressive tissue-specific ^{18}F -FDG uptake (Figure 1F). Focal ^{18}F -FDG uptake corresponded to the spleen, S.Int., and L.Int. and was in agreement with the statistically significant temporal trend observed in the terminal ex vivo biodistribution study. Changes in focal uptake of ^{18}F -FDG were observed in the intestines as early as day 3 after infection. Although it is generally challenging to distinguish between early- and late-stage infection in this acute model, interestingly, one animal had higher median ^{18}F -FDG uptake in the intestinal area at day 3 than the other two and did not survive to day 4 (Supplemental Figure 1A).

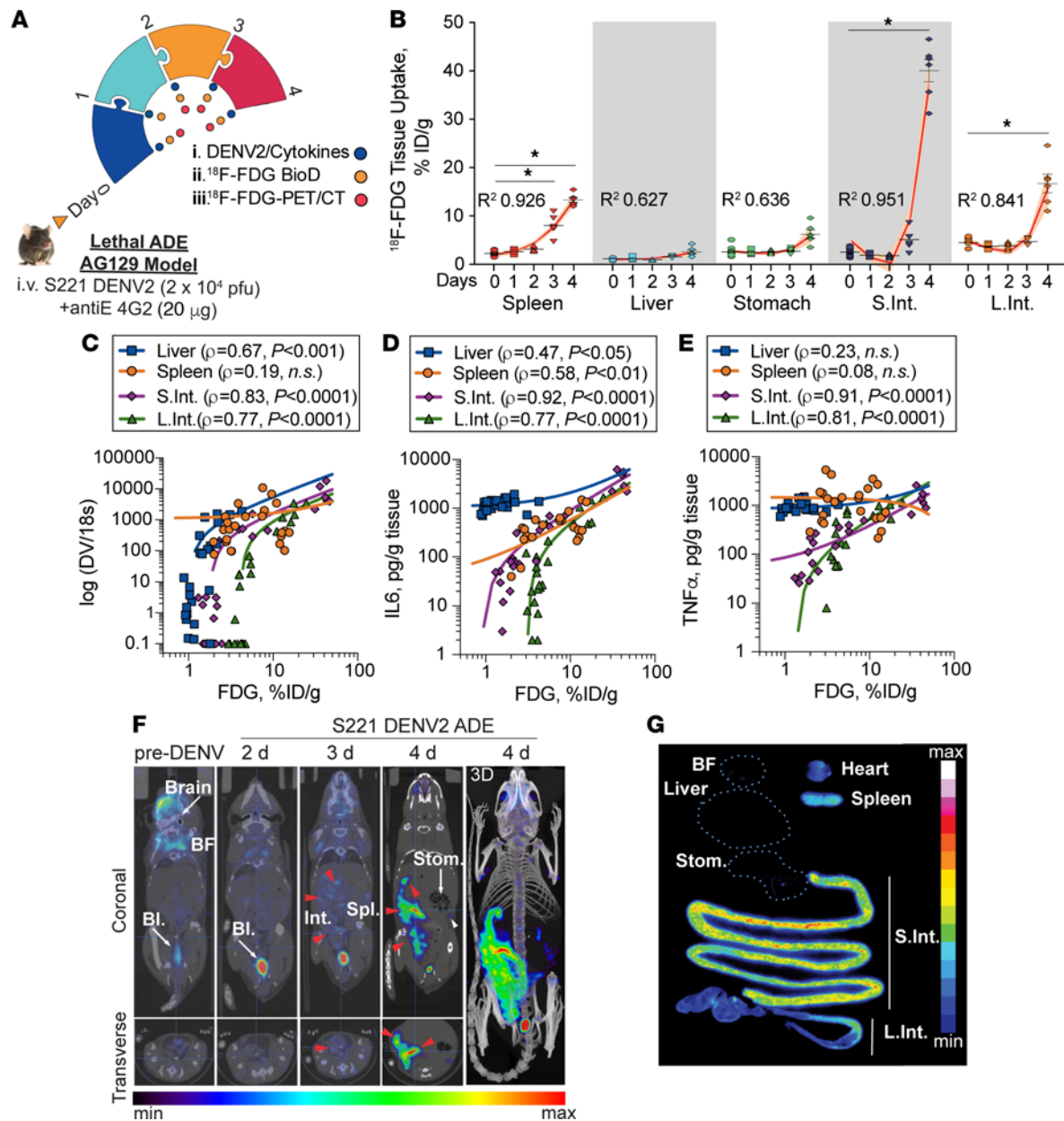


Figure 1. Serial ^{18}F -FDG tissue analysis and PET/CT imaging to understand dynamic evolution of inflammatory foci in lethal mouse-adapted S221 DENV2 model. (A) Schematic representation of induction of mouse-adapted S221 DENV2 lethal immune complex infection at day 0, and timing of biomarker measurements (DENV2/cytokines, postmortem ^{18}F -FDG tissue biodistribution [BioD], and ^{18}F -FDG-PET/CT) over course of disease in female AG129 mice. (B) Terminal ^{18}F -FDG biodistribution in selected tissues plotted over time. Circles, squares, triangles, inverted triangles, and diamonds represent individual tissue uptake at days 0, 1, 2, 3, and 4, respectively ($n = 6$ –12 mice/group). For spleen and small and large intestine (S.Int. and L.Int.), significant ^{18}F -FDG uptake was observed relative to naive mice (as represented at $t = 0$ day). Mean ^{18}F -FDG uptake was compared by 2-way ANOVA with multiple comparisons; $*P < 0.001$. Fractional polynomial regression curves, estimated from second- or first-order fractional polynomial regression models, are shown for the nonlinear time course of ^{18}F -FDG uptake following disease progression. Beige shading indicates the 95% CI around the fitted line in red, with R^2 values shown. Regression curves were plotted in STATA. (C–E) Tissue biodistribution of ^{18}F -FDG uptake (%ID/g) plotted against paired values for concentrations of (C) DENV, (D) IL-6, and (E) TNF- α levels in mice after infection. Points represent individual tissues ($n = 96$ mice) from mice with active disease in the spleen (orange), liver (blue), S.Int. (purple), L.Int. (green); $n = 24$ mice/tissue respectively. A linear regression model of terminal ^{18}F -FDG uptake versus other biomarkers is shown for selected tissues, and Spearman's ρ and P values are shown. (F) ^{18}F -FDG-PET/CT images of progressing inflammatory lesions following i.v. ^{18}F -FDG administration (representative data shown from 1 animal of a cohort of $n = 3$). The images show increasing uptake in spleen (Spl.) and intestines (Int.) over time (white and red arrowheads, respectively). Brown fat (BF), bladder (Bl.) CT images show substantial gaseous accumulation within the stomach (Stom.). (G) Ex vivo autoradiography of whole tissue mounts immediately following the day 4 ^{18}F -FDG-PET/CT of same mouse as in F, with the highest uptake observed in the S.Int. and lower uptake observed in the L.Int., spleen, and heart. No appreciable ^{18}F -FDG signal was observed in the Stom., liver, and BF. Dotted lines represent the boundaries of the tissues with no discernible uptake (representative data shown from 1 animal of a cohort of $n = 4$).

This suggests an inflection point in disease trajectory that may predict disease severity. Furthermore, day 4 CT images reveal observable distention in the abdomen, likely due to bloating from gaseous build up in the stomach. To further explore ^{18}F -FDG uptake, we employed microdistribution at a tissue-specific level, utilizing digital autoradiography (DAR). DAR evaluation of whole-tissue mounts at day 4 after infection revealed that the majority of the targeted tissue uptake within the intestinal tract was confined to the S.Int. (Figure 1G and Supplemental Figure 1B). Dramatically lower DAR signal was observed in the stomach, brown fat, and heart when compared with the S.Int. in infected mice. DAR showed no appreciable liver ^{18}F -FDG uptake and confirmed *in vivo* ^{18}F -FDG-PET/CT observations.

Taken together, the data for this preclinical model suggest that ^{18}F -FDG levels in the S.Int. and L.Int. may be used as a prognostic biomarker that reflects the time course of dengue disease progression and, moreover, shows convergent validity in terms of correlation with previously known biomarkers of dengue disease.

^{18}F -FDG uptake is effectively suppressed with antiviral therapy in the mouse-adapted DENV2 lethal model. Although celgosivir, an α -glucosidase inhibitor, was protective against DENV in AG129 mice (21, 22, 27), a phase Ib randomized placebo-controlled clinical trial in Singapore failed to show significant reduction of viremia (10, 12). Our follow-up preclinical study reveals the challenges in lowering viral load when drug treatment is initiated near peak viremia, comparable to how most patients present clinically (11). Since severe dengue usually develops after resolution of the viremic phase (28), an alternative endpoint that is directly associated with disease severity is desirable for assessing antiviral drug efficacy. Taking advantage of the robust capability of ^{18}F -FDG to detect DENV-mediated inflammation in the S.Int., as validated in Figure 1, we next assessed its value as a predictive biomarker of antiviral therapy response. Mice were treated with celgosivir 4 times daily (q.i.d.; 50 mg/kg), following the regimen that has been shown to improve celgosivir efficacy in mice (11) (Figure 2A). The treatment completely protected mice from lethal infection with S221 when dosing commenced on day 2 after infection (Figure 2B). It is worth noting that a significant drop in viremia (33-fold) was already observed at day 4 after infection ($P = 0.03$) (Figure 2C). Tissue analysis of S221 infection showed significant reduction of viral load in the livers, stomachs, S.Int., and L.Int. of treated mice as compared with that of untreated mice on day 4 after infection (Supplemental Figure 2A). Significant reduction of cytokine production was induced: TNF- α was induced in the S.Int. and IL-6 was induced in stomach, S.Int., L.Int., and spleen (Supplemental Figure 2, B and C). Terminal biodistribution studies showed that ^{18}F -FDG uptake in the S.Int. of treated mice was trending toward reduction compared with treatment-naïve mice as early as day 1 after treatment (i.e., 3 days after infection). By day 2 after treatment (i.e., 4 days after infection), significantly dramatic reductions ($P < 0.0001$) in ^{18}F -FDG uptake, compared with treatment-naïve mice, were observed in the spleen (1.85-fold), liver (2.08-fold), stomach (2.45-fold), S.Int. (5.24-fold), and L.Int. (3.16-fold) (Figure 2D and Supplemental Figure 2D). To apply the ^{18}F -FDG-PET/CT imaging paradigm for monitoring treatment response in DENV, we performed longitudinal imaging in mice treated with celgosivir. Importantly, we did not observe accumulation of ^{18}F -FDG at the anticipated intestinal area by ^{18}F -FDG/PET in celgosivir-treated mice at day 2 after infection, as compared with treatment-naïve mice (Figure 2E, Supplemental Figure 2D, and Supplemental Figure 3). This suggests that ^{18}F -FDG-PET/CT can visualize tissue-specific host response to antiviral treatments in dengue when using the mouse-adapted S221 DENV2 strain.

Nonlethal or lethal infection of mice with a DENV2 clinical isolate correlates with intestinal ^{18}F -FDG uptake. The DENV2 S221 lethal infection model was used for initial validation of ^{18}F -FDG uptake because of the previous demonstration that focal inflammation and increased viral load in the intestinal region are the principal contributors to the pathology and ultimate lethality (20). Next, we wanted to determine if ^{18}F -FDG uptake was sufficiently sensitive as a biomarker to distinguish between nonlethal primary (virus alone, Figure 3A) and lethal antibody-enhanced infection (ADE infection, Figure 3B) using a clinical strain of DENV2 (DENV2-3295 [EDEN2]), as we described previously in the AG129 mouse model (11, 29). Examination of the kinetics of viral load in the serum (Figure 3C) revealed no difference in RNA genome equivalent copies between nonlethal infection versus lethal ADE infection with EDEN2 DENV2. This is despite 80% mortality of mice by day 5 after infection in the latter group (Figure 3D). This was not the case when RNA genome equivalent copy levels were tested in other tissues. A parallel analysis on day 4 after infection, revealed significantly higher levels of RNA genome equivalent copies in the S.Int., L.Int., and livers of ADE-infected animals (5.85-, 1.94-, and 53.5-fold, respectively, $P < 0.005$; Supplemental Figure 4A). The spleen only showed differential viral load at day 3 after infection (1.87-fold, $P < 0.001$). Notably, TNF- α and IL-6 levels were prominently distinguishable in the S.Int.

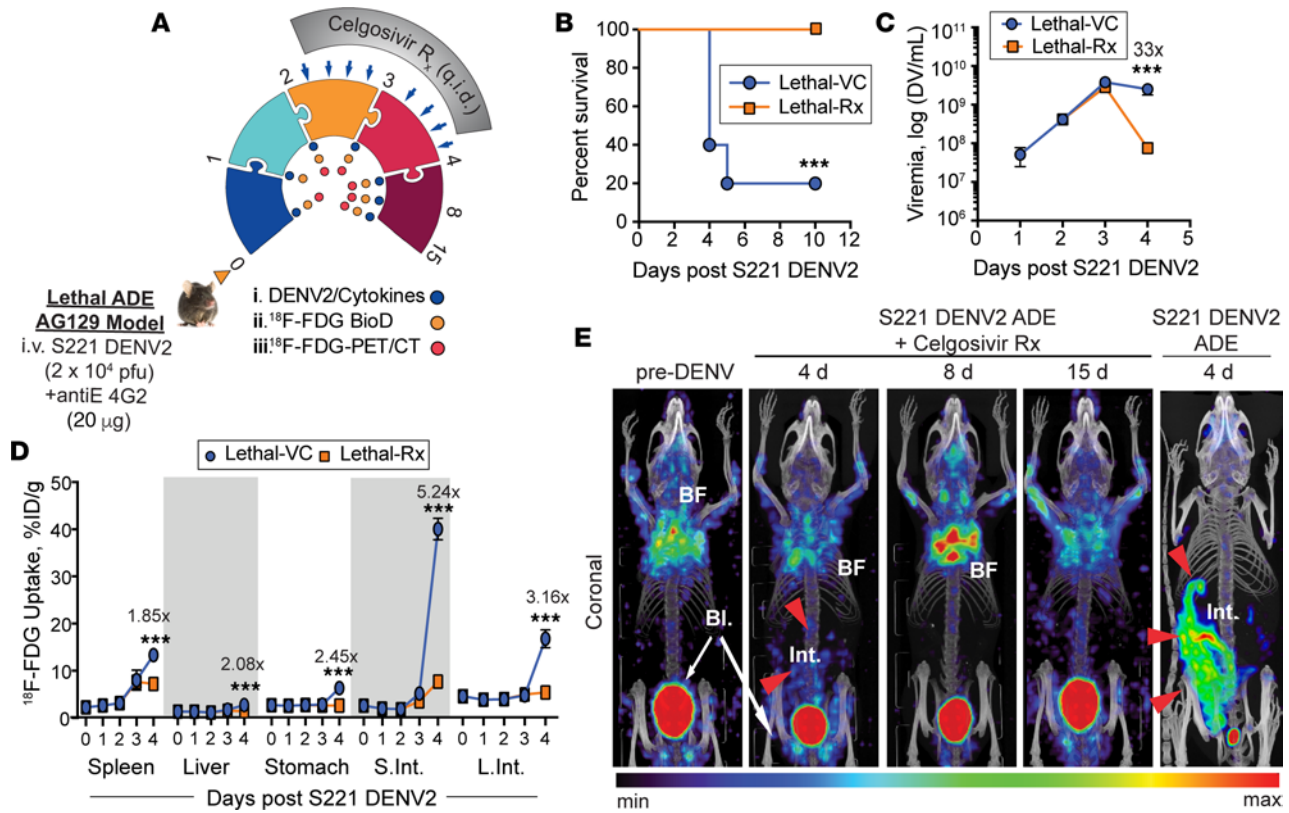


Figure 2. ¹⁸F-FDG-PET/CT imaging to monitor the response to antiviral treatment following lethal infection with mouse-adapted S221 DENV2. (A) Schematic representation of the antiviral treatment regimen for celgosivir 4 times daily (q.i.d.) at day 2 after initiation of lethal S221 DENV2 infection. Treatment time course is indicated by blue arrows. Biomarkers (DENV2/cytokines, ¹⁸F-FDG tissue biodistribution (BioD), and ¹⁸F-FDG-PET/CT) were sampled over course of treatment. (B) Survival curves of lethal-infected mice following treatment with vehicle control (i.e., treatment naive; *n* = 12 mice/group, blue circles) and celgosivir q.i.d. (*n* = 6 mice/group, orange squares) at day 2 after DENV2. Results are representative of 2 independent experiments. Kaplan-Meier curves were compared by Mantel-Cox log-rank test; ****P* = 0.045. (C) Celgosivir-treated mice showed significant differences in viremia versus the treatment-naive group at day 4 after infection by PCR assay (*n* = 6-12 mice/group). Mean values were compared by 2-way ANOVA with multiple comparisons; ****P* = 0.03. (D) Terminal ¹⁸F-FDG uptake by BioD in selected tissues plotted over time after infection. Significant ¹⁸F-FDG uptake was observed in the treatment group compared with the treatment-naive group at day 4 after infection, with fold reduction indicated above data points. Mean values were compared by 2-way ANOVA with multiple comparisons; ****P* < 0.001. (E) ¹⁸F-FDG-PET/CT images before and during antiviral treatment with celgosivir showing dramatically lower ¹⁸F-FDG uptake in the gut region as compared with treatment-naive mice (far right panel) (representative data shown from 1 animal of a cohort of *n* = 3). VC, vehicle control; Rx, treatment.

(2.49- and 17.36-fold, respectively, *P* < 0.05) and L.Int. (2.51- and 5.28-fold, respectively, *P* < 0.001) in ADE infection compared with nonlethal primary infection at day 4 after infection (Supplemental Figure 4, B and C). As observed for S221 ADE infection, the liver showed no appreciable changes in TNF- α and IL-6 levels when nonlethal primary and ADE infection with the EDEN2 clinical isolate were compared. While differences in serum levels of IL-6 were significant at day 4 after infection when comparing disease severity, TNF- α serum levels were not. This similarly reflects the situation in which reliable prognostic markers, blood-based or otherwise, for predicting severe dengue are lacking or are severely limited.

Mapping of ¹⁸F-FDG tissue uptake by terminal biodistribution studies showed a consistent and prominent tissue-specific uptake pattern in the spleen, S.Int., and L.Int., for both nonlethal primary and lethal ADE infection with the EDEN2 strain (Figure 3, E-G). The validity of ¹⁸F-FDG, as a potential dengue infection biomarker, was further supported by its ability to identify temporal infection-induced inflammation changes in the S.Int. and L.Int. as early as 3 days after infection in the EDEN2 ADE model (Figure 3E). This is in contrast to the virus and IL-6 levels; both displayed tissue-specific changes no earlier than 4 days after infection (Supplemental Figure 4). TNF- α only showed differences between nonlethal and lethal groups in two tissues. Temporal changes in ¹⁸F-FDG uptake were prominent in the S.Int. and L.Int. in the lethal EDEN2 ADE infection model relative to the nonlethal primary infection model (4.13- and 4.03-fold at day 3 after infection, respectively, *P* < 0.0001).

When ^{18}F -FDG tissue uptake was normalized to baseline (localization ratio [LR]) in noninfected mice, the metabolic activities across a wider range of tissue compartments were independent and dynamic between nonlethal primary infection (Figure 3F) and lethal ADE infection groups (Figure 3G). Additionally, lethal EDEN2 ADE infection showed an enhanced LR in the kidneys at day 4 after infection (3.4-fold) and a markedly higher LR in the S.Int. on day 3 (7.5-fold), day 4 (11.1-fold), and day 5 (5.5-fold) after infection. The ^{18}F -FDG LR of the heart, a major organ of metabolic activity under normal physiological conditions, exhibited an inconsistent uptake pattern, which is likely not reflective of infection pathology. ^{18}F -FDG uptake and LR in the 15 organs sampled is shown in Supplemental Table 2, A–D.

Next, we followed individual treatment-naive and celgosivir-treated mice temporally by ^{18}F -FDG-PET/CT imaging using the lethal EDEN2 ADE infection model (Figure 3, H and I). ^{18}F -FDG-PET/CT imaging results (Figure 3H) showed a similar trend to that obtained for lethal ADE infection with S221 mouse-adapted virus (Figure 1F), in which inflammation foci were detected primarily in the intestinal region. Yet, as early as day 2 after infection, ^{18}F -FDG biodistribution studies in EDEN2 ADE infection model showed marked prominent intestinal uptake. By day 4 after infection, mice were moribund if not treated with an anti-dengue agent. In fact, initiation of q.i.d. celgosivir treatment on day 2 after infection showed a marked reduction in intestinal ^{18}F -FDG uptake by PET on day 4 after infection and no abnormal ^{18}F -FDG uptake in the lower abdominal area for up to day 15 after infection (Figure 3I). Quantitative distribution profiles, from serial in vivo PET/CT images of ^{18}F -FDG, compared tracer uptake in the entire gut region of interest (ROI, not including the stomach, heart, and bladder) of treatment-naive and celgosivir-treated ADE-infected mice. Time activity curves within gut ROIs for each mouse, showed a trend toward increased gut uptake for treatment-naive mice (M1–M6) compared with the treated mice (M7–M9) (Figure 3J). By day 3, ^{18}F -FDG gut uptake was significantly increased in the treatment-naive arm, compared with earlier time points or compared with the treated arm on the same day ($P < 0.05$). There was a 1.73-fold higher gut uptake in the treatment-naive mice versus drug-treated mice by day 3 ($P < 0.05$). By day 4, the difference was more prominent, with a 3.95-fold increase, because two treatment-naive mice (M5 and M6) that survived showed ^{18}F -FDG gut uptake on day 3 that was significantly higher than that on the preceding day ($P < 0.0001$). Overall, as desired for a predictive biomarker for treatment response, the ^{18}F -FDG uptake in the celgosivir-treated group was stable over time at around the baseline level. Hence, our data suggest that a threshold of ^{18}F -FDG gut uptake can forecast infection trajectory and severity as well as therapeutic benefit and survival outcome.

Discussion

The broad range of clinical symptoms during dengue infection and the lack of precision in grading dengue severity have made the task of correlating biomarkers, such as serum viral load or secreted levels of virus-encoded nonstructural protein 1 (NS1), with pathologies in target tissues difficult. There are no biomarkers that can sensitively distinguish viral load reduction due to innate cellular antiviral response from the viral load reduction due to antiviral drug-mediated mechanisms. This has been a considerable impediment for the development of new antiviral drugs (12) and therapeutic antibodies (30) against dengue. To address this gap, we hypothesized that (a) ^{18}F -FDG-PET imaging can provide a noninvasive, real-time approximation for monitoring DENV-mediated inflammation in vivo and that (b) this approach can monitor the efficacy of novel therapeutic compounds that can directly target the major tissues involved in dengue pathogenesis.

Increased cytokine production is one of the hallmarks of dengue infection. The “cytokine storm,” with its accompanying inflammation and vasculopathy, is thought to play a critical role in disease severity (13). Several studies have reported the association of disease severity with increased levels of serum proinflammatory cytokines/chemokines, such as TNF- α , IL-4, IL-6, IL-8, IL-10, IFN- γ , and MIP-1 (31–34). However, none of these cytokines qualify as a robust biomarker of disease severity. Our previous study using the AG129 mouse model in a setting that mimicked primary infection in human infants with circulating maternal DENV antibodies showed a correlation of disease severity with TNF- α and IL-6 levels in the S.Int. This was not recapitulated in serum samples that were tested in parallel (20).

Recently, two independent studies reported the potential for the virus-encoded NS1 protein to directly contribute to dengue disease pathogenesis (35, 36). The study by Modhiran and colleagues (35, 36) demonstrated that NS1 is a pathogen-associated molecular pattern that recognizes TLR4 in target cells, which can lead to release of proinflammatory cytokines. The study by Beatty and colleagues (35, 36) showed that NS1

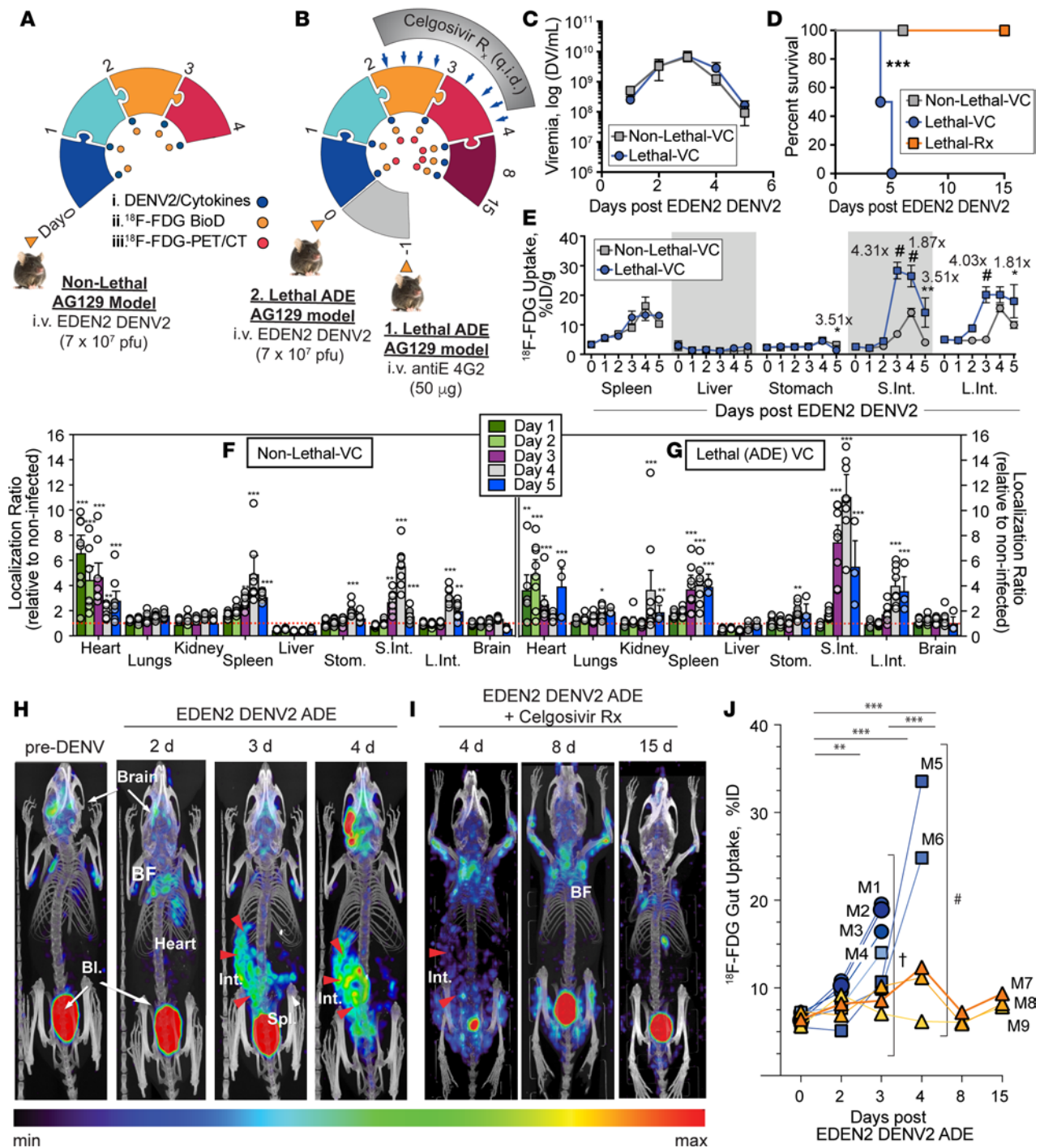


Figure 3. Detection of ¹⁸F-FDG following nonlethal or lethal infection with DENV2 clinical isolate EDEN2 identifies differences in infection severity and intestinal disease amelioration. Schematic diagram of experimental setup in (A) nonlethal and (B) lethal ADE infection. (C) Viremia measured in treatment-naive (vehicle control-treated) nonlethal- and lethal-infected mice by PCR assay ($n = 3-8$ mice/group; gray squares and blue circles, respectively). (D) Survival curves of nonlethal- and lethal-infected mice following treatment with vehicle control ($n = 8$ mice/group) and lethal-infected mice treated with celgosivir q.i.d. ($n = 6$ mice/group, orange squares) at day 2 after DENV2. Results are representative of 2 independent experiments. Celgosivir treatment significantly enhanced mouse survival in the lethal model. Kaplan-Meier curves were compared by Mantel-Cox log-rank test; *** $P < 0.0001$. (E) ¹⁸F-FDG uptake (%ID/g) in selected tissues plotted over time after EDEN2 infection ($n = 3-8$ mice/group). Significant ¹⁸F-FDG uptake was observed in the lethal group compared with nonlethal group as early as day 3 after infection, with fold difference indicated between groups above data points. Mean values were compared by 2-way ANOVA with multiple comparisons; * $P < 0.05$; ** $P < 0.001$. (F and G) Expanded tissue profile of ¹⁸F-FDG uptake normalized to ¹⁸F-FDG profile in noninfected mice (localization ratio [LR]) and plotted over time in (F) nonlethal and (G) lethal EDEN2-infected mice. For spleen, S.Int., L.Int., and, in one instance, the kidney, significant ¹⁸F-FDG uptake is observed relative to naive mice (LR = 1, represented as red dashed line). Mean values were compared by 2-way ANOVA with multiple comparisons; * $P < 0.05$; ** $P < 0.01$; *** $P < 0.0001$ ($n = 3-8$ mice/group). (H and I) Posterior 3D volume rendering of fused ¹⁸F-FDG-PET/CT scans of DENV2 progression in mice (H) following lethal EDEN2 infection and (I) after induction of celgosivir therapy 2 days after infection (representative data shown from 1 animal of a cohort of $n =$

6 treatment naive and $n = 3$ celgosivir treated). (J) Analysis of in vivo longitudinal ^{18}F -FDG-PET/CT images from individual mice (M1–M9) focused on ^{18}F -FDG gut concentrations (%ID) in treatment-naive (M1–M6, blue squares) and celgosivir-treated (M7–M9, yellow triangles) arms. Mean values were compared by 2-way ANOVA with multiple comparisons; between group means at individual time points, $^1P < 0.05$; $^*P < 0.0001$; over disease time course within group, $^{**}P < 0.01$; $^{***}P < 0.0001$. VC, vehicle control; Rx, treatment.

alone can promote permeability in pulmonary endothelial cells using an in vitro Transwell assay and in vivo in the AG129 mouse model. Importantly, a dose-dependent release of proinflammatory cytokines, such as IL-6 and TNF- α , was observed in the S.Int. of the AG129 mouse model (35, 36) in these studies. These observations support the present study, irrespective of whether AG129 mice were infected with a mouse-adapted strain (17) or clinical isolate of DENV2 (11). In our study, ^{18}F -FDG accumulated preferentially in the intestines and correlated with indicators of disease severity that are associated with inflammation. The liver has been implicated in numerous studies of DENV infection in humans and mouse models (17, 37, 38), and, indeed, hepatomegaly was observed in our lethal mouse model. However, very low ^{18}F -FDG liver accumulation was detected, which corresponded to the low levels of proinflammatory cytokines produced in the organ during DENV infection in our studies (3). The consistently normal inflammatory status of the liver over the course of disease, despite measurable viral load, is surprising and warrants further studies.

The use of the reduction of serum viremia as the primary laboratory endpoint for evaluating therapeutics against DF failed to show any significant efficacy, as recent clinical trials of repurposed drugs have demonstrated (10, 39–42). Moreover, the potency of the tested drugs has been significantly questioned, since analysis showed an almost 4-log reduction in viral load during the acute phase for both the treated and untreated arms (10, 39–42). Viremia clearance is associated with the immune status of the patients and virus serotype (39, 43). In the case of adult patients, viremia reduction during secondary infection is significantly faster than that for primary infection (10, 12, 39), most probably due to the rapid reactivation of the acquired immune system. Overall, the wide variation of the viremia reduction rate, coupled with the short window given to observe these changes in patients, hampers the assessment of statistical difference among drug-treated and drug-naive cases. Our recent study in AG129 mice showed differing kinetics of viral load in different tissues that, notably, did not always correlate with serum viremia (20). Therefore, we hypothesized that if a drug can decrease viral load in a tissue where viral burden directly correlates with disease severity, then it is conceivable that it may prevent patients from progressing to severe dengue and death. In this respect, the robust preclinical validation of increased proinflammatory cytokine levels and virus infection with focal ^{18}F -FDG tissue uptake, particularly the S.Int., represents an essential first step for developing this tool as a potential clinical endpoint measurement for proof-of-concept assessment of drug efficacy in patients.

To our knowledge, such research is not being pursued elsewhere in the context of dengue, even though the value of tracking inflammation through ^{18}F -FDG-PET for acute viral diseases has been discussed for flu virus in both ferret and human models of infection (44, 45). However, one recent case study reported an incidental ^{18}F -FDG-PET imaging in an adult male with DF with detectable serum viremia during an annual cancer screening (46). Abnormal ^{18}F -FDG uptake was observed in the spleen and lymph nodes of this patient when compared with scans obtained 1 year later at follow-up. Notably, ^{18}F -FDG uptake appeared to show an increase in the intestine during DF, although the authors did not comment on this (46). In this preclinical report, we suggest that the in vivo quantification of ^{18}F -FDG uptake in tissues of pathological interest (i.e., S.Int.) in our rodent models is grossly underestimated. This assumption can be largely attributed to the challenge in delineating a volume of uptake due to insufficient soft tissue contrast in CT and the very compact anatomy of the mouse. However in the clinical setting, the liver could serve as a reasonable reference region for in vivo ^{18}F -FDG-PET assessments, given the consistent tracer uptake irrespective of dengue disease severity. Regardless, using the simple PET/CT volumetric measurements used in this study, we still see appreciable group differences in global gut volume uptake, which includes the S.Int., L.Int., spleen, and mesentery.

As the global burden of dengue continues to rise, with nearly 400 million infections each year and more than two-thirds of the world's population at risk of infection, therapeutic interventions are urgently required. DHF and DSS, caused by DENV, are life-threatening severe diseases with mortality of up to 20% (1), and there remain many unanswered questions regarding the disease pathogenesis. Therefore, there is an urgent need to develop translational clinical platforms that will allow further understanding of disease pathophysiology and response to investigational treatments that will benefit patients.

In summary, our studies in mouse models of DENV infection show increased ^{18}F -FDG-PET uptake in the intestinal tract that correlates with increased inflammatory cytokines levels and viral load in that tissue. ^{18}F -FDG-PET intensity in the intestinal tract is also responsive to drug treatment, which, therefore, can be monitored noninvasively over time. The quantifiable reduction in intestinal ^{18}F -FDG uptake by PET/CT imaging strongly supports that this approach can be used to noninvasively and robustly define inflammation reduction as a surrogate endpoint for drug efficacy during preclinical development and clinical validation. Generally, drug development is an arduous and expensive undertaking, even more so for acute diseases caused by dengue, Zika, and other related viruses, when the low-profit margin is a further impediment to drugs reaching the market. The approach we take may have a profound effect on reducing the high costs of drug discovery for emerging infectious diseases through reduced trial size and fast tracking of the drug development process. Hence, clinical trials centered on ^{18}F -FDG-PET imaging of dengue patients during acute DF will be required to fully define the parameters for noninvasively identifying inflammatory foci.

Methods

Cells, virus, and antibodies. BHK-21 cells (baby hamster kidney fibroblast cells, ATCC) were cultured in RPMI1640 medium (Gibco) supplemented with 10% FBS and 1% penicillin/streptomycin (P/S) at 37°C in 5% CO_2 . C6/36, an *Aedes albopictus* cell line (ATCC), was maintained in RPMI1640 medium with 10% FBS, 25 mM HEPES, and 1% P/S at 28°C in the absence of CO_2 . The mouse-adapted strain DENV2 S221 (47) was a gift from Sujana Shrestha (La Jolla Institute for Allergy and Immunology). EDEN2 (GenBank accession EU081177.1) was obtained from the Early Dengue infection and outcome study in Singapore (29). Virus strains were grown in C6/36 cells, and the supernatants were stored at -80°C after filtration through a 0.45- μm membrane. Virus titer was determined by standard plaque assay on BHK-21 cells. mAb 4G2 (mouse IgG2_a, anti-E of all serotypes) hybridoma was purchased from ATCC and isolated as previously described (20).

Virus infection and drug treatment in mice. Sv/129 mice deficient in type I and II IFN receptors (AG129 mice), purchased from B&K Universal, were housed in the BSL-2 animal facility at Duke-NUS Medical School. Seven- to eleven-week-old mice were used for all in vivo experiments. For virus-mAb 4G2 immune complex infection, 2×10^4 pfu S221 (100 μl) was mixed with 20 μg 4G2 mAb (100 μl) for 1 hour on ice and inoculated i.v. in a total volume of 200 μl into mice (20). For nonlethal EDEN2 infection, 7×10^7 pfu of virus was inoculated i.v. into mice. ADE infection (lethal) of AG129 mice was achieved by injecting 50 μg of 4G2 mAb into mice 1 day prior to EDEN2 infection by i.v. inoculation with 7×10^7 pfu of virus. Celgosivir (an α -glucosidase inhibitor), stored at 100 mg/ml in PBS at -30°C , was diluted with PBS to a final concentration of 1 mg/200 μl (50 mg/kg/mouse) before each dosing and administered orally into mice with a q.i.d. regimen (3 doses every 4 hours followed by 1 single dose for a 12-hour cycle), starting on day 2 after DENV infection.

Ex vivo biodistribution studies. At 1, 2, 3, 4, and 5 days after DENV infection, mice were injected with approximately 1 MBq (27 μCi) ^{18}F -FDG (Singapore Radiopharmaceuticals Pte. Ltd.) via the tail vein. After a 75-minute uptake phase, the mice were sedated using 2% Isoflurane (Piramal Healthcare), and blood was collected via cardiac puncture. The mice were subsequently euthanized, and various organs (heart, lungs, thyroid, liver, pancreas, stomach, mesenteric lymph nodes, kidneys, muscle, bone, brain, spleen, tail, S.Int., L.Int., contents of stomach, contents of S.Int., contents of L.Int., and remaining carcass) were harvested, weighed, and placed in tubes separately. After collection, the tubes were measured for tissue radioactivity (^{18}F , 1 minute per sample) on a gamma counter (2480 Wizard², Perkin Elmer) with decay-correction together with input dose tubes. The counts were then normalized to %ID/g (measured radioactivity per gram brain tissue/injected radioactivity), and data were reported as mean \pm SEM of $n = 6$ –12 per group, or normalized to tissue uptake pre-DENV2 infection (i.e., baseline or day 0) and reported as LR.

In vivo PET. For each specific scan, mice were injected i.v. with 15–30 MBq (~ 400 –800 μCi) ^{18}F -FDG (100 μl). After the 75-minute uptake phase, the mice were sedated using 1.5%–2% Isoflurane (Piramal Healthcare) and placed in the prone position in a heat-regulated mouse bed. A total body PET/CT scan was acquired using the VECTor⁴CT (MILabs). The PET scan was acquired in list mode in 2 frames lasting 20 minutes each, using the HE-UHR mouse 0.7-mm pinhole collimator. The PET scan was immediately followed by a total body CT (75-mm FOV) on spiral mode acquired at full scan angle and in normal step mode (tube current, 0.24 mA; tube voltage, 50 kV). The CT and the PET image data sets were reconstructed using the MILabs reconstruction software (version 3.09). The CT raw data (≈ 720 projections) were reconstructed by filtered back projection at 80- μm voxel size. The acquired PET

images were defined with the following signal/background parameters: 445.5 keV (minimum) to 544.5 keV (maximum), with 495.0 keV (central peak) as the photopeak representing ^{18}F -signal and flanking windows 425.7 keV (minimum) to 445.5 keV (maximum), with 435.5 keV (central peak), as well as 544.5 keV (minimum) to 564.3 keV (maximum), with 554.4 keV (central peak) as background. The resulting photopeak counts were reconstructed using a maximum likelihood expectation maximization algorithm (12 iterations, 0.8-mm voxel size, 12 subsets), and a Gaussian filter was applied (1 mm 3D). PET images were then coregistered and attenuation corrected with CT data with the same reconstruction software.

3D image processing and ROI analysis. Image display and analysis was done using PMOD software v.3.704 (PMOD Technologies). Coronal and transverse image slices containing the overall highest PET voxel intensities in the gut were chosen specifically for displaying disease progression across the different days at approximately similar anatomical regions midway through the ventral-dorsal axis and just proximal to the bladder. PET image voxels were scaled, so all images across cohorts could be displayed, reflecting similar levels of radioactivity. Maximum intensity projections were generated to display overall ^{18}F -FDG distribution throughout the animal body, with the CT minimum and maximum intensities set at about 10% and 80%, respectively, to limit visualization to the mouse skeletal structure.

Due to the expansion of the gut volume during disease progression and the poor contrast of internal organs in the rodent abdomen, ROI definition was done on the CT image by approximating the entire abdominal cavity. ROIs were conservatively deformed to avoid ^{18}F -FDG hotspots, such as the bladder and the heart. The CT-guided ROI was then applied to the coregistered PET image. Quantification of ROIs was conducted with a built-in statistics tool, in which intensity was converted to uptake and normalized to injected dose.

DAR. Immediately following ^{18}F -FDG-PET/CT imaging, mice were euthanized, and the following organs were harvested approximately 2 hours after injection of ^{18}F -FDG: brown fat, heart, liver, spleen, stomach, S.Int., and L.Int. Control pre-DENV-infected mice were injected with similar doses to those used in ^{18}F -FDG-PET studies, and tissues were harvested 2 hours after tracer administration. The organs were covered with plastic wrap and whole mounted in a cassette (Select Cassette). Organs were exposed for 5 minutes to the phosphoscreen (Phosphor Screen BAS-IP MS 2040 E, GE Lifesciences). The screen was scanned at a 10- μm resolution on a phosphorimager (Typhoon FLA 9500, GE Life Sciences). Digital images generated were further processed as 16-bit images using ImageJ (1.48v, NIH).

Quantification of viral load in serum and tissues by reverse transcription quantitative real-time PCR. Blood samples were collected each day for up to 5 days after infection by submandibular bleeding, and serum samples were used to measure viral copy number by quantitative real-time PCR (qRT-PCR) as described previously (20). Tissues were collected and snap frozen in liquid nitrogen after removal of all visible luminal content from stomach and intestines. Frozen tissues were then homogenized using mortar and pestle with <1 g sea sand (Merck Millipore) in PBS, and, after centrifugation, the supernatants were used to measure tissue viral load and cytokine levels. For the viral load measurement, RNA was extracted from the supernatants using the Trizol extraction method and subjected to RT-PCR as described previously (20). The values of viral genome numbers in tissues were normalized to the expression level of 18s ribosomal RNA (18s).

Measurement of tissue cytokines. The levels of cytokines (TNF- α and IL-6) in serum and tissue homogenates were measured by using Ready-SET-Go! ELISA kits (eBioscience) according to the manufacturer's instructions.

Statistics. Kaplan-Meier survival curves were assessed for significance using the Mantel-Cox log-rank test to compare treatment-naive and drug-treatment groups. Two-way ANOVA was used to compare several groups, followed by the Holm-Sidak post-hoc procedure for multiple comparison test; family-wise significance and confidence level were considered statistically significant at $P < 0.05$. Data are presented as mean \pm SEM, unless otherwise noted. Statistical analysis and graphing were performed with Prism 7 software (GraphPad Software).

The nonlinear time course of ^{18}F -FDG uptake was fitted using second- or first-order fractional polynomial regression models (48) in STATA12.1 (StataCorp). Tests for differences in deviance were used to decide whether to use first- or second-order fractional polynomials and were also used to compare the best fitting fractional polynomials against linear trend and no trend.

Study approval. All animal studies were performed in full compliance with policies and procedures approved by the SingHealth IACUC (Singapore) and conformed to NIH guidelines and public law.

Author contributions

AMC, SW, SK, JGHL, and SGV designed the research. AMC, SW, KJH, JYT, JO, MR, and RMFS performed the experiments. AMC, SW, JYT, and SGV designed the figures. AMC, SW, KJH, SK, and SGV obtained ethical approval for the study. AMC, SW, KJH, JYT, and YBC analyzed the data and conducted the statistical analyses. AMC, SW, YBC, and SGV wrote the manuscript. All authors edited the manuscript.

Acknowledgments

These studies were funded by Duke-NUS start-up funds (to AMC), National Medical Research Council/Open Fund — Young Individual Research Grant/0003/2016 (to SW), the Duke-NUS Khoo Pilot Award (to SK), National Medical Research Council/Clinical Trial Grant Co-Development Scheme/0001/2015 (to JGHL), and National Medical Research Council/Cooperative Basic Research Grant/0103/2016 (to SGV). We thank Eng Eong Ooi (Duke-NUS Medical School) and Harald Groen (MILabs, Netherlands) for helpful discussions.

Address correspondence to: Ann-Marie Chacko or Subhash G. Vasudevan, Duke-NUS Medical School, 8 College Road, Singapore 169857. Phone: 65.6601.1671; E-mail: ann-marie.chacko@duke-nus.edu.sg (A.M. Chacko). Phone: 65.6516.6718; E-mail: subhash.vasudevan@duke-nus.edu (S.G. Vasudevan).

- Guzman MG, Harris E. Dengue. *Lancet*. 2015;385(9966):453–465.
- Fauci AS, Morens DM. Zika virus in the Americas — yet another arbovirus threat. *N Engl J Med*. 2016;374(7):601–604.
- Fink J, Gu F, Vasudevan SG. Role of T cells, cytokines and antibody in dengue fever and dengue haemorrhagic fever. *Rev Med Virol*. 2006;16(4):263–275.
- Halstead SB. Dengue. *Lancet*. 2007;370(9599):1644–1652.
- Gubler DJ. Dengue/dengue haemorrhagic fever: history and current status. *Novartis Found Symp*. 2006;277:3–16.
- Simmons CP, Farrar JJ, Nguyen vV, Wills B. Dengue. *N Engl J Med*. 2012;366(15):1423–1432.
- Hadinegoro SR, et al. Efficacy and long-term safety of a dengue vaccine in regions of endemic disease. *N Engl J Med*. 2015;373(13):1195–1206.
- Halstead SB, Russell PK. Protective and immunological behavior of chimeric yellow fever dengue vaccine. *Vaccine*. 2016;34(14):1643–1647.
- Aye KS, et al. Pathologic highlights of dengue hemorrhagic fever in 13 autopsy cases from Myanmar. *Hum Pathol*. 2014;45(6):1221–1233.
- Low JG, et al. Efficacy and safety of celgosivir in patients with dengue fever (CELADEN): a phase 1b, randomised, double-blind, placebo-controlled, proof-of-concept trial. *Lancet Infect Dis*. 2014;14(8):706–715.
- Watanabe S, Chan KW, Dow G, Ooi EE, Low JG, Vasudevan SG. Optimizing celgosivir therapy in mouse models of dengue virus infection of serotypes 1 and 2: The search for a window for potential therapeutic efficacy. *Antiviral Res*. 2016;127:10–19.
- Sung C, et al. Extended Evaluation of Virological, Immunological and Pharmacokinetic Endpoints of CELADEN: A Randomized, Placebo-Controlled Trial of Celgosivir in Dengue Fever Patients. *PLoS Negl Trop Dis*. 2016;10(8):e0004851.
- Martina BE, Koraka P, Osterhaus AD. Dengue virus pathogenesis: an integrated view. *Clin Microbiol Rev*. 2009;22(4):564–581.
- Ferreira RA, et al. Circulating cytokines and chemokines associated with plasma leakage and hepatic dysfunction in Brazilian children with dengue fever. *Acta Trop*. 2015;149:138–147.
- Chan KW, Watanabe S, Kavishna R, Alonso S, Vasudevan SG. Animal models for studying dengue pathogenesis and therapy. *Antiviral Res*. 2015;123:5–14.
- Balsitis SJ, et al. Lethal antibody enhancement of dengue disease in mice is prevented by Fc modification. *PLoS Pathog*. 2010;6(2):e1000790.
- Zellweger RM, Prestwood TR, Shresta S. Enhanced infection of liver sinusoidal endothelial cells in a mouse model of antibody-induced severe dengue disease. *Cell Host Microbe*. 2010;7(2):128–139.
- Tan GK, Ng JK, Trasti SL, Schul W, Yip G, Alonso S. A non mouse-adapted dengue virus strain as a new model of severe dengue infection in AG129 mice. *PLoS Negl Trop Dis*. 2010;4(4):e672.
- Ng JK, et al. First experimental in vivo model of enhanced dengue disease severity through maternally acquired heterotypic dengue antibodies. *PLoS Pathog*. 2014;10(4):e1004031.
- Watanabe S, Chan KW, Wang J, Rivino L, Lok SM, Vasudevan SG. Dengue virus infection with highly neutralizing levels of cross-reactive antibodies causes acute lethal small intestinal pathology without a high level of viremia in mice. *J Virol*. 2015;89(11):5847–5861.
- Schul W, Liu W, Xu HY, Flamand M, Vasudevan SG. A dengue fever viremia model in mice shows reduction in viral replication and suppression of the inflammatory response after treatment with antiviral drugs. *J Infect Dis*. 2007;195(5):665–674.
- Watanabe S, et al. Dose- and schedule-dependent protective efficacy of celgosivir in a lethal mouse model for dengue virus infection informs dosing regimen for a proof of concept clinical trial. *Antiviral Res*. 2012;96(1):32–35.
- Hillner BE, et al. The impact of positron emission tomography (PET) on expected management during cancer treatment: findings of the National Oncologic PET Registry. *Cancer*. 2009;115(2):410–418.
- Vaidyanathan S, Patel CN, Scarsbrook AF, Chowdhury FU. FDG PET/CT in infection and inflammation—current and emerging clinical applications. *Clin Radiol*. 2015;70(7):787–800.
- Brust D, et al. Fluorodeoxyglucose imaging in healthy subjects with HIV infection: impact of disease stage and therapy on pat-

- tern of nodal activation. *AIDS*. 2006;20(7):985–993.
26. Spier BJ, Perlman SB, Jaskowiak CJ, Reichelderfer M. PET/CT in the evaluation of inflammatory bowel disease: studies in patients before and after treatment. *Mol Imaging Biol*. 2010;12(1):85–88.
27. Rathore AP, et al. Celgosivir treatment misfolds dengue virus NS1 protein, induces cellular pro-survival genes and protects against lethal challenge mouse model. *Antiviral Res*. 2011;92(3):453–460.
28. Nisalak A, Halstead SB, Singharaj P, Udomsakdi S, Nye SW, Vinijchaikul K. Observations related to pathogenesis of dengue hemorrhagic fever. 3. Virologic studies of fatal disease. *Yale J Biol Med*. 1970;42(5):293–310.
29. Low JG, et al. Early Dengue infection and outcome study (EDEN) - study design and preliminary findings. *Ann Acad Med Singap*. 2006;35(11):783–789.
30. Robinson LN, et al. Structure-guided design of an anti-dengue antibody directed to a non-immunodominant epitope. *Cell*. 2015;162(3):493–504.
31. Green S, et al. Elevated plasma interleukin-10 levels in acute dengue correlate with disease severity. *J Med Virol*. 1999;59(3):329–334.
32. Raghupathy R, et al. Elevated levels of IL-8 in dengue hemorrhagic fever. *J Med Virol*. 1998;56(3):280–285.
33. Butthep P, Chunhakan S, Yoksan S, Tangnararatchakit K, Chuansumrit A. Alteration of cytokines and chemokines during febrile episodes associated with endothelial cell damage and plasma leakage in dengue hemorrhagic fever. *Pediatr Infect Dis J*. 2012;31(12):e232–e238.
34. Bozza FA, et al. Multiplex cytokine profile from dengue patients: MIP-1beta and IFN-gamma as predictive factors for severity. *BMC Infect Dis*. 2008;8:86.
35. Beatty PR, Puerta-Guardo H, Killingbeck SS, Glasner DR, Hopkins K, Harris E. Dengue virus NS1 triggers endothelial permeability and vascular leak that is prevented by NS1 vaccination. *Sci Transl Med*. 2015;7(304):304ra141.
36. Modhiran N, et al. Dengue virus NS1 protein activates cells via Toll-like receptor 4 and disrupts endothelial cell monolayer integrity. *Sci Transl Med*. 2015;7(304):304ra142.
37. Paes MV, et al. Liver injury and viremia in mice infected with dengue-2 virus. *Virology*. 2005;338(2):236–246.
38. Seneviratne SL, Malavige GN, de Silva HJ. Pathogenesis of liver involvement during dengue viral infections. *Trans R Soc Trop Med Hyg*. 2006;100(7):608–614.
39. Tricou V, et al. A randomized controlled trial of chloroquine for the treatment of dengue in Vietnamese adults. *PLoS Negl Trop Dis*. 2010;4(8):e785.
40. Tam DT, et al. Effects of short-course oral corticosteroid therapy in early dengue infection in Vietnamese patients: a randomized, placebo-controlled trial. *Clin Infect Dis*. 2012;55(9):1216–1224.
41. Nguyen NM, et al. A randomized, double-blind placebo controlled trial of balapiravir, a polymerase inhibitor, in adult dengue patients. *J Infect Dis*. 2013;207(9):1442–1450.
42. Whitehorn J, et al. Lovastatin for the Treatment of Adult Patients With Dengue: A Randomized, Double-Blind, Placebo-Controlled Trial. *Clin Infect Dis*. 2016;62(4):468–476.
43. Duyen HT, et al. Kinetics of plasma viremia and soluble nonstructural protein 1 concentrations in dengue: differential effects according to serotype and immune status. *J Infect Dis*. 2011;203(9):1292–1300.
44. Jonsson CB, et al. Molecular imaging reveals a progressive pulmonary inflammation in lower airways in ferrets infected with 2009 H1N1 pandemic influenza virus. *PLoS ONE*. 2012;7(7):e40094.
45. Shirone N, et al. Axillary lymph node accumulation on FDG-PET/CT after influenza vaccination. *Ann Nucl Med*. 2012;26(3):248–252.
46. Jinguji M, Kajiya Y, Nakajo M, Nakajo M, Yoshiura T. Increased 18F-FDG uptake in the spleen and multiple lymph nodes in dengue fever. *Clin Nucl Med*. 2016;41(5):e255–e256.
47. Yauch LE, et al. A protective role for dengue virus-specific CD8+ T cells. *J Immunol*. 2009;182(8):4865–4873.
48. Royston P, Altman DG. Regression Using Fractional Polynomials of Continuous Covariates: Parsimonious Parametric Modelling. *J R Stat Soc Ser C Appl Stat*. 1994;43(3):429–467.